

See discussions, stats, and author profiles for this publication at: <http://www.researchgate.net/publication/256798389>

Monodisperse Spindle-Like FeWO₄ Nanoparticles: Controlled Hydrothermal Synthesis and Enhanced Optical Properties

ARTICLE *in* JOURNAL OF SOLID STATE CHEMISTRY · DECEMBER 2012

Impact Factor: 2.13 · DOI: 10.1016/j.jssc.2012.07.026

CITATIONS

6

READS

28

6 AUTHORS, INCLUDING:



Jinxue Guo

Qingdao University of Science and Technol...

33 PUBLICATIONS 244 CITATIONS

SEE PROFILE



Monodisperse spindle-like FeWO_4 nanoparticles: Controlled hydrothermal synthesis and enhanced optical properties

Jinxue Guo, Xiaoyu Zhou, Yibin Lu, Xiao Zhang*, Shaoping Kuang*, Wanguo Hou

Qingdao University of Science & Technology, College of Chemistry and Molecular Engineering, No.53, Zhengzhou Road, People's Republic of China, Qingdao, Shandong 266042, China

ARTICLE INFO

Article history:

Received 26 April 2012

Received in revised form

9 July 2012

Accepted 11 July 2012

Available online 20 July 2012

Keywords:

FeWO_4

Monodisperse

Hydrothermal synthesis

Photocatalysis

Crystal growth

ABSTRACT

Monodisperse FeWO_4 nanoparticles with specific spindle-like morphology have been synthesized in the presence of citric acid through hydrothermal process. In the synthesis route, citric acid played four roles such as the reducing agent, chelating reagents, structure-directing agent and stabilizing agents. In addition, the morphology of FeWO_4 was dramatically tuned by the pH value of the precursor medium. The optical properties of FeWO_4 were investigated with UV–Vis spectra and photoluminescence spectroscopy. The photocatalytic experiments demonstrated that the decomposition efficiency of the monodisperse spindle-like FeWO_4 nanoparticles is 74% after 30 min of UV irradiation, which displayed remarkable enhanced photodegradation activity compared with ordinary FeWO_4 sample (57%) and normal TiO_2 photocatalysts P-25 (56%).

© 2012 Elsevier Inc. All rights reserved.

1. Introduction

Monodisperse particles, especially uniform monodisperse nanoparticles with specific shape and size have attracted increasing interest because of their significant catalytic, biological, ceramic, mechanical, optical and magnetic properties [1–6]. Thus, a number of methods such as Sol–Gel, precipitation, microwave-assisted, hydrothermal, solvothermal, templating, top–down and microfluidic synthesis have been employed for the synthesis of monodisperse particles [7–14]. Among them, hydrothermal method is one of the suitable methods for synthesis of nanoparticles since the preparation conditions, such as pH value, temperature, composition of precursor and application of template, are easily tunable [15–17].

In recent years, metal tungstates have been on the focus of intensive research due to their high application potential in various fields such as photoluminescence, optical fibers, scintillator materials, humidity sensors, magnetic properties and catalysis [18–21]. As one of the important families of inorganic materials, FeWO_4 has been proven to display significant magnetic and optical properties [22,23]. Many efforts have been made for the synthesis of FeWO_4 with various morphologies such as hierarchical plate, nanorods and hierarchical microstructures [15,23–25]. It is well known that the electrical, magnetic, optical and some other properties of inorganic nanoparticles greatly depend on their particle size and shape, but pursuing a rational solution pathway for assembling individual atoms into special microstructures is still a challenge. Penn et al.

have proposed a new growth mechanism termed as “oriented attachment” [26]. In this crystal growth progress, the adjacent small primary nanoparticles are self-assembled into bigger particles by sharing a common crystallographic orientation, in which the surface free energy is lower than other crystallographic orientations. As the absorption of ion or surfactant molecular on the crystallographic surface could change its free energy, the surfactant-assisted hydrothermal method has been selected for the synthesis of novel FeWO_4 microstructures through the oriented attachment progress.

In this paper, we reported an effective surfactant-assisted hydrothermal method for the preparation of monodisperse FeWO_4 nanoparticles with uniform spindle shape-specific for the first time. The possible crystal growth mechanism has been proposed. The optical properties were examined with photoluminescence spectra (PL). UV–Vis spectra were employed to estimate the band gap energy of monodisperse spindle-like FeWO_4 nanoparticles. In addition, the photodegradation of methyl orange (MO) was conducted to investigate the photocatalytic activities of monodisperse spindle-like FeWO_4 nanoparticles under UV irradiation. It is indicated that monodisperse spindle-like FeWO_4 nanoparticles exhibit an excellent photocatalytic performance.

2. Experimental

All chemicals were of analytical grade and were used as purchased without further purification. $\text{Na}_2\text{WO}_4 \cdot 4\text{H}_2\text{O}$, $\text{FeSO}_4 \cdot 7\text{H}_2\text{O}$, citric acid and NaOH were all obtained from Shanghai Chemical Reagent Company. Deionized water was used throughout.

* Corresponding authors. Fax: +86 532 84022681.
E-mail address: zhx1213@126.com (X. Zhang).

FeWO₄ products were prepared via a hydrothermal synthesis method. The typical hydrothermal progress of monodisperse spindle-like FeWO₄ nanoparticles was presented as follows: FeSO₄·7H₂O (0.01 M) and citric acid (0.01 M) were mixed together in 50 mL of deionized water to get a jade-green solution. The stoichiometric amount of Na₂WO₄·4H₂O was dissolved into another 50 mL of deionized water. The Na₂WO₄·4H₂O solution was added into the FeSO₄·7H₂O and citric acid solution with magnetic stirring. After the pH value of the mixed solution was tuned to be 7 with NaOH (1 M) solution, the color of the solution became bottle-green. Then the resulting homogeneous solution was transferred into Teflon-lined stainless-steel autoclaves. The autoclave was sealed and maintained at 180 °C for 24 h, and cooled to room temperature naturally. The obtained brown products were collected and washed with absolute ethanol and deionized water several times to remove impurities, and they were dried at 80 °C for 4 h.

In order to estimate the effect of pH values, the FeWO₄ products obtained from different precursor with pH values such as 6.5, 7.5 and 8 were synthesized for comparison. And the experiment following the same synthesis route of spindle-like samples but without citric acid was designed to investigate the influence of citric acid on the morphology of final FeWO₄ products.

The samples obtained under different experimental conditions were characterized with X-ray powder diffraction (XRD), scanning electron micrographs (SEM), transmission electron micrographs (TEM) and other techniques. XRD was recorded by a Philips X'pert X-ray diffractometer in the 2θ range from 10° to 60° with Cu K_α radiation (λ=1.5418 Å). SEM images were obtained with a JEOL JSM-6700F scanning electron microscope. TEM and selected area electron diffraction (SAED) patterns were taken on a JEOL JEM-1200EX transmission electron microscope. High-resolution TEM (HRTEM) analysis was performed with a FEI TECNAI F30. PL spectra were measured with a Hitachi F-2700 Fluorescence Spectrophotometer at room temperature.

The photocatalytic activities of FeWO₄ samples were evaluated in the process of the degradation of MO in an aqueous solution under UV irradiation of a 10 W UV lamp. Before the photocatalytic test, the obtained FeWO₄ samples were irradiated under UV light for 24 h to remove the remains of surfactant. The reaction cell was placed in a sealed black box. In each experiment, the aqueous suspension of MO (100 mL, 10 mg/L) containing 100 mg photocatalyst was dispersed in a vessel. Before exposure to UV light irradiation, the suspension was continuously stirred for 3 h in the dark to ensure that adsorption/desorption equilibrium had been reached. The concentration of MO during the degradation was analyzed with Hitachi U-3010 UV-Vis spectrophotometer at 464 nm every 10 min.

3. Results and discussion

3.1. Characterization of monodisperse spindle-like FeWO₄ nanoparticles

The typical powder XRD pattern of as-prepared monodisperse spindle-like FeWO₄ nanoparticles was shown in Fig. 1. It is shown that all diffraction peaks of the spindle-like FeWO₄ nanoparticles can be indexed to a pure, well-crystalline, monoclinic wolframite tungstate structure with lattice parameters of *a*=4.739 Å, *b*=5.718 Å, *c*=4.965 Å, which are in good agreement with the reported values (PDF 46-1446). There is no other impurity peaks appeared in Fig. 1, indicating the high purity of the products prepared through this progress. Moreover, the good crystallization of the obtained FeWO₄ nanoparticles is proven by the strong and sharp reflection peaks of the XRD pattern.

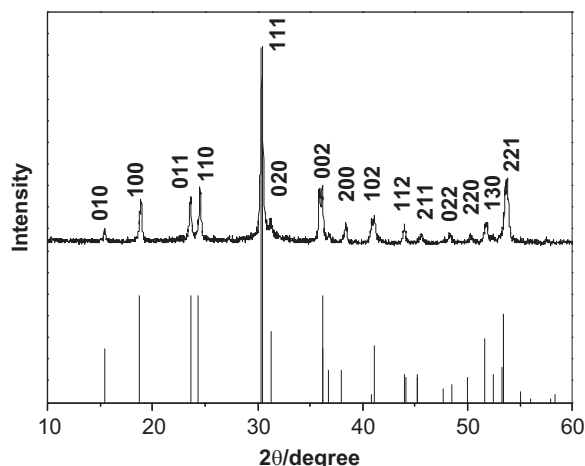


Fig. 1. XRD patterns of monodisperse spindle-like FeWO₄ nanoparticles.

The low-magnification SEM images of the as-obtained products were shown as the images a and b in Fig. 2, which clearly indicates that the products are composed of uniform spindle-like nanoparticles. As is displayed in these images, all these spindle-like nanoparticles are monodisperse particles with equatorial diameters of ca. 150–200 nm and lengths ranging from ca. 250 nm to 400 nm. As is shown in the TEM image of Fig. 2c, the surfaces of these monodisperse spindle-like nanoparticles are not smooth but rough. The single spindle-like FeWO₄ nanoparticles are composed of smaller aggregated nanoparticles, which can be further testified by higher magnification SEM image in Fig. 2e. This result indicates that these spindle-like nanoparticles possess high surface area and potentially have many defects. The selected area electron diffraction (SAED) pattern on the spindle-like nanoparticles was recorded and shown in Fig. 2d. It is revealed that the prepared precipitate is well-crystalline, which agrees well with the results of XRD. Interestingly, the SAED pattern suggests that the spindle-like nanoparticles, which are made of smaller particles, also exhibit a single crystalline property.

The pH value of the precursor medium is a crucial factor on the morphology of the products. Thus, controlled experiments have been carried out to investigate the influence of pH value on the morphology of final FeWO₄ crystals. SEM images a–d in Fig. 3 revealed the morphology evolution of resultant FeWO₄ nanostructures obtained from different precursor pH values after hydrothermal treatment at 180 °C for 24 h. Obviously, the morphology of FeWO₄ nanostructures can be tailored by adjusting the pH values of the precursor medium, which was filled into the autoclave. When pH value was 6.5, the as-prepared FeWO₄ crystals are nanoparticles with diameters of several tens nanometers (Fig. 3a). When the pH value was increased to 7.0, monodisperse spindle-like morphology of FeWO₄ could be obtained as shown in Fig. 3b. As is shown in Fig. 3c, the products retain their spindle-like morphology when the pH value was 7.5. But the boundaries of these spindle-like FeWO₄ nanoparticles are unclear, and the particles combine with each other, which are marked with white arrows in Fig. 3c. When the pH value was adjusted to 8.0, the products are large quantities of irregular aggregates and no spindle-like particles are visible (Fig. 3d).

Besides pH values, other influencing factors such as the introduction of surfactant can also tune the samples' morphology. To declare the effect of surfactant citric acid on the morphology of the final FeWO₄ particles, different samples have been prepared by adjusting the hydrothermal synthesis process with and without surfactant. As is shown in Fig. 3e, there are no monodisperse spindle-like FeWO₄ nanoparticles detected without the addition

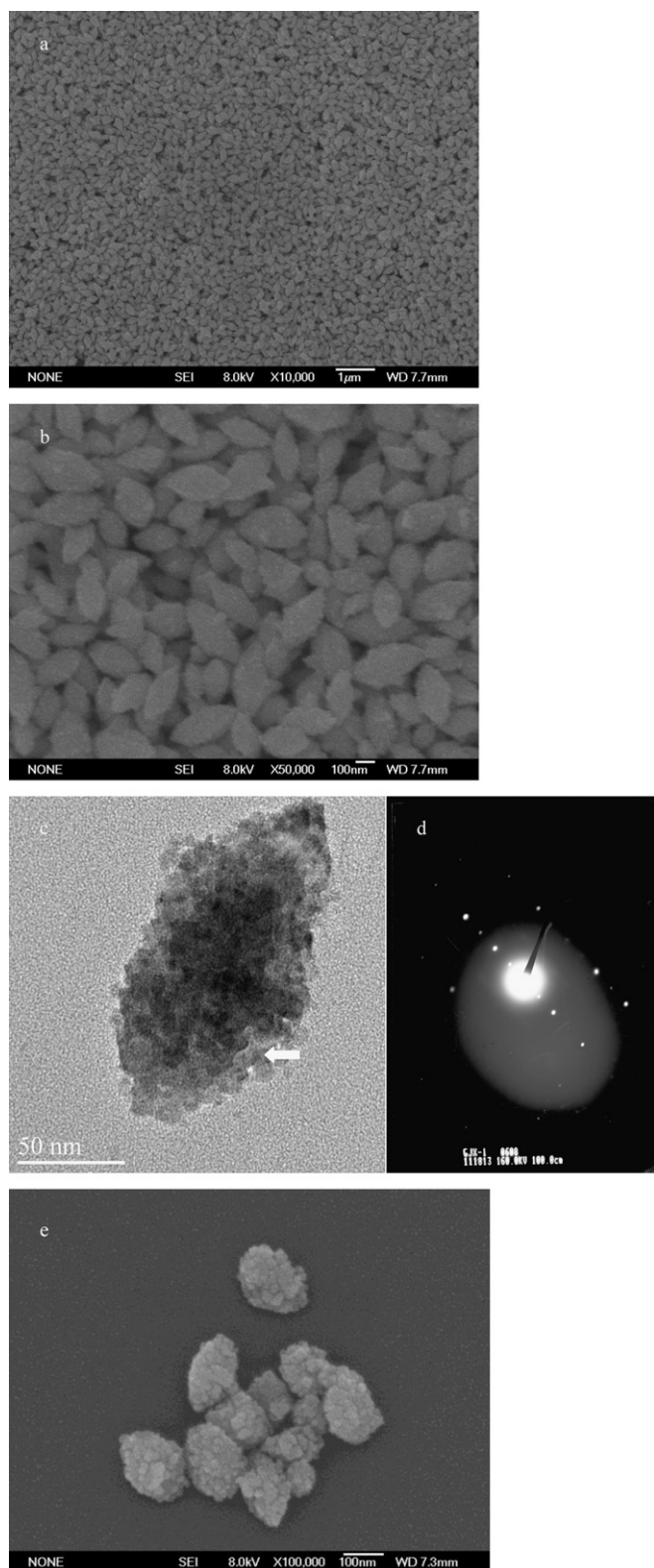


Fig. 2. SEM images and TEM images of monodisperse spindle-like FeWO_4 nanoparticles prepared hydrothermally at 180°C for 24 h in the presence of citric acid. (a, b) low-magnification SEM images; (c) TEM images, (d) the SAED pattern recorded from the fringe indicated by the white arrow and (e) high-magnification SEM image.

of citric acid. The FeWO_4 nanoparticles agglomerate severely, which indicated that citric acid acted as stabilizing agent for the synthesis of monodisperse spindle-like nanoparticles by adsorbance on their surface.

TEM and HRTEM observations have been carried out to determine the crystal orientation and declare the microstructure of the spindle-like nanoparticles. As is shown in the HRTEM image of Fig. 4a, the spindle-like nanoparticles with rough surface are composed of primary nanoparticles, which is consistent with the conclusion drawn from the SEM images. Fig. 4b depicts the enlarged lattice-resolved HRTEM images of the area marked with white ellipse in Fig. 4a, which indicates that the product is well crystallized and exhibits a clear crystal lattice. The interplanar spacing of the observed lattice planes could be finely detected as about 0.565 nm, 0.505 nm and 0.385 nm, which are consistent with the spacings for the (0 1 0), (0 0 1) and (0 1 1) planes of the monoclinic phase FeWO_4 , respectively. The parallelism and overlap of the lattice fringes observed along the same crystallographic directions suggests the oriented attachment growth mechanism of the products. As is proposed by Penn and Banfield [26], when the attachment occurred between two or more nanoparticles, they would share a common crystallographic orientation and join at the planar interface. The area marked with white rectangle in Fig. 4a is the attachment area of two nanoparticles. An enlarged lattice-resolved HRTEM image was recorded for this area and shown in Fig. 4c. The broken line denotes the boundary of the adjacent two nanocrystals. The lattice planes at the planar interface between two nanocrystals could be determined to be 0.385 nm, which depicts that this region is structurally uniform with an oriented crystallographic direction. The same crystal lattice value observed at the planar interface of two nanocrystals suggests that the attached building nanoparticles share the same crystal direction. So the single crystal-line property of spindle-like nanoparticles which is approved by the SAED pattern is understandable.

3.2. Possible growth mechanism

The actual formation mechanism of monodisperse spindle-like FeWO_4 nanoparticles is not distinct. But on the basis of the above-mentioned experimental observations, we present a oriented self-assembly progress accompanying Ostwald ripening for the possible growth process, which is shown in Scheme 1.

Initially, Fe^{2+} was stabilized by the adherent of citric acid to make a homogeneous solution. When the WO_4^{2-} was added into the solution, the citric acid could prevent the formation of FeWO_4 nuclei. In the hydrothermal progress, citric acid acted as reducing agent to prevent the oxidation of Fe^{2+} by the oxygen left in the autoclave. When the hydrothermal treatment time went on, the temperature of the solution increased. Chelation between the Fe^{2+} and citric acid would become weak and the WO_4^{2-} would replace citric acid to form FeWO_4 nuclei. In order to lower the surface energy, the FeWO_4 nuclei grew up into nanocrystals through self-assembly growth mechanism. In the HRTEM image, the parallelism and overlap of the lattice fringes are observed along the same crystallographic directions. According to this result, the FeWO_4 nanocrystals in the solution preferred to aggregate with each other in (0 1 1) planes based on the oriented attachment growth mechanism. We believed that citric acid played the key role in the oriented attachment crystal growth progress. Murphy has claimed that the preferential adsorption of molecules and ions onto different crystal facets directed the growth of particles into various shapes by controlling the growth rates along different crystal axes [27]. In the present sample, the nanocrystals attached to each other along the (0 1 1) plane at the planar interface sharing the same crystal direction. It is indicated that the surface energy of the (0 1 1) plane is different from the surface energies of (0 1 0) and (0 0 1) planes. The citric acid preferred to adsorb onto the (0 1 0) and (0 0 1) planes, preventing facet-to-facet crystal aggregation along these planes with an electrostatic inhibition, which would lead to preferential attachment of the nanocrystals along the (0 1 1) plane. However, the spindle-like morphology would not form when the pH values changed slightly. It is indicated that there is a strong

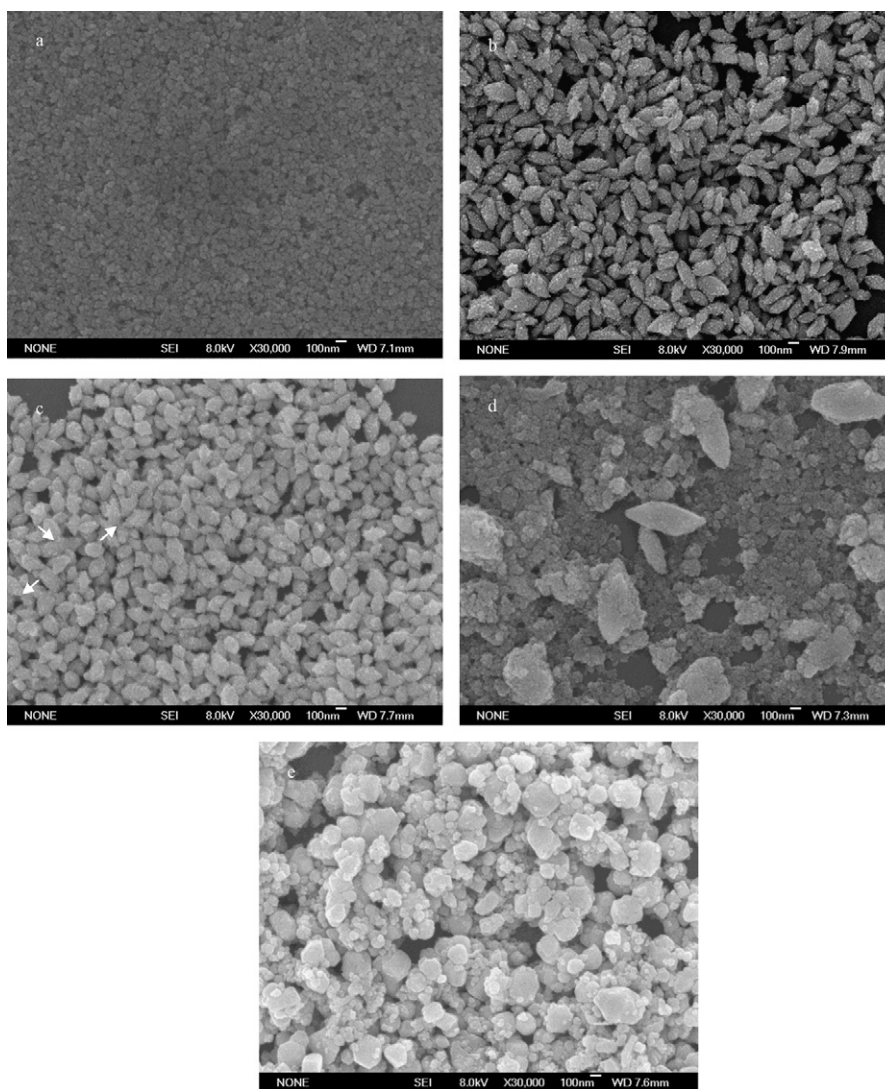


Fig. 3. SEM images of FeWO_4 crystallites prepared hydrothermally at 180°C for 24 h in the presence of citric acid: (a) $\text{pH}=6.5$, (b) $\text{pH}=7$, (c) $\text{pH}=7.5$, (d) $\text{pH}=8$; and the absence of citric acid: (e) $\text{pH}=7$.

competitive effect between citric acid and OH^-/H^+ , which would result in anisotropic crystal growth and be disadvantageous to morphologically controlled growth of FeWO_4 . Once the spindle particles formed, the citric acid absorbed on their surface acted as stabilizing agents to prevent the aggregation of monodisperse particles. Finally, the continuous growth of FeWO_4 evolved into single crystalline spindle-like nanoparticles through the Ostwald ripening progress with prolonged reaction time.

Based on the above analyses, the directing growth of FeWO_4 nuclei chelated with citric acid is proposed in the starting period. Subsequently, the oriented self-assembly attachment along the particular direction might lead to the formation of spindle-like architectures. In this period, the change of pH values could tune the growth direction of the nanocrystals. With the hydrothermal time prolonging, the Ostwald ripening process will result in fully developed crystals.

3.3. Optical properties and photocatalytic activity

The optical properties of these spindle-like FeWO_4 nanoparticles were examined with UV–Vis spectra. The results are shown in Fig. 5. As is demonstrated in Fig. 5, FeWO_4 showed a shoulder absorption at 340 nm, which can be identified as tungstate group.

For an indirect gap semiconductor, the optical band gap energy of FeWO_4 can be calculated with the following formula:

$$(\alpha h\nu)^2 = K(h\nu - E_g)$$

In this formula, α is the absorption coefficient, K is the characteristic constant of semiconductors, $h\nu$ and E_g are photo energy and optical band gap energy, respectively. According to the equation, $(\alpha h\nu)^2$ has a linear relation with the $h\nu$. The E_g values of FeWO_4 were thus determined by extrapolation of the linear relation to $(\alpha h\nu)^2 = 0$. As is illustrated in the inset of Fig. 5, the band gap of monodisperse spindle-like FeWO_4 nanoparticles is estimated to be about 2.17 eV. This value is narrower than the indirect band gap of 2.59 eV for hexangular FeWO_4 architectures and slightly wider than 2.0 eV for bulk FeWO_4 [25–28], that might be due to the effect of the morphology and particle size of the monodisperse spindle-like particles.

Room-temperature photoluminescence spectra of the FeWO_4 samples have also been examined with the excitation line at 300 nm. Fig. 6 contains the PL spectra of FeWO_4 products obtained at pH 7 and pH 8, respectively. As is shown in Fig. 6, pure spindle-like FeWO_4 nanoparticles obtained at pH 7 display a blue emission band in the range of 420–520 nm with two strong peaks centered at about 452 nm and 469 nm (curve a). Compared

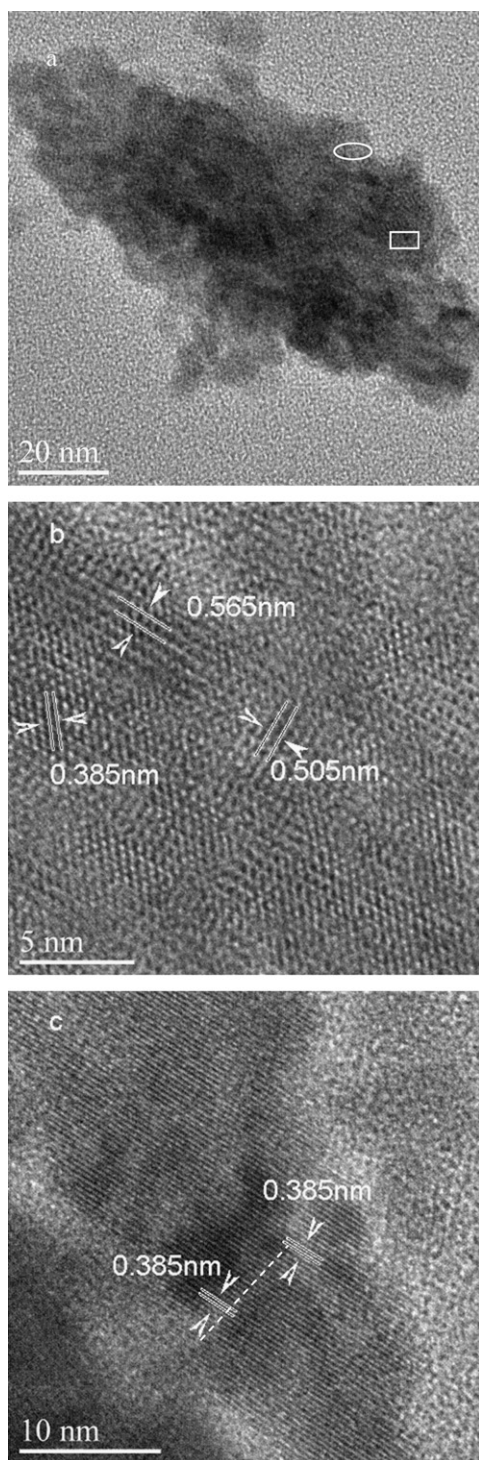


Fig. 4. (a) TEM image of a typical spindle-like FeWO_4 nanoparticles, (b, c) HRTEM images of the two areas marked with the ellipse and rectangle, respectively.

with the PL spectra of spindle-like FeWO_4 nanoparticles, the position of the emission peaks of the irregular nanoparticles, which were obtained at pH 8, remained almost unchanged (curve b). The spectral characteristics of FeWO_4 are very similar to those of other scheelite tungstate crystals MWO_4 ($\text{M}=\text{Pb}, \text{Ca}, \text{Ba}, \text{Sr}$), which consist of two emission components [29]. It is revealed that the emission intensity of emission peaks at 452 nm shows no obvious difference between these two kinds of samples. The blue emission peaks around 450 nm (2.75 eV) is ascribed to the regular lattice center, which is affected with the crystallization. The same luminescence intensity indicates that crystallization of these two samples are good, which is in good agreement with the conclusion approved by the XRD pattern and SAED. However, at the position of 469 nm, the absolute luminescence intensity of spindle-like FeWO_4 nanoparticles is higher than that of products obtained at pH 8. The emission intensity at the position of 470 nm (2.64 eV) has been understood as a defect-related emission. The higher intensity of the peak at 470 nm indicated that spindle-like FeWO_4 nanoparticles possess higher surface area and more defects than the products obtained at pH 8, which is a positive factor for the photocatalytic properties.

MO molecules, a widely used dye, were selected as the representative pollutant for the photocatalytic efficiency test of the as-prepared spindle-like FeWO_4 nanoparticles. Temporal changes in the concentration of MO have been monitored by examining the variation of the maximal absorption band at about 464 nm. Under UV irradiation of a 10 W UV lamp, its temporal evolution of spectral changes in the process of the photodegradation of MO was displayed with white hollow circles in Fig. 7a. There is a gradual decrease of MO absorption at the wavelength of 464 nm under the irradiation of UV light. The absorption peaks corresponding to MO completely disappeared after about 50 min. In addition, the color of the dyes solution changed from initial red

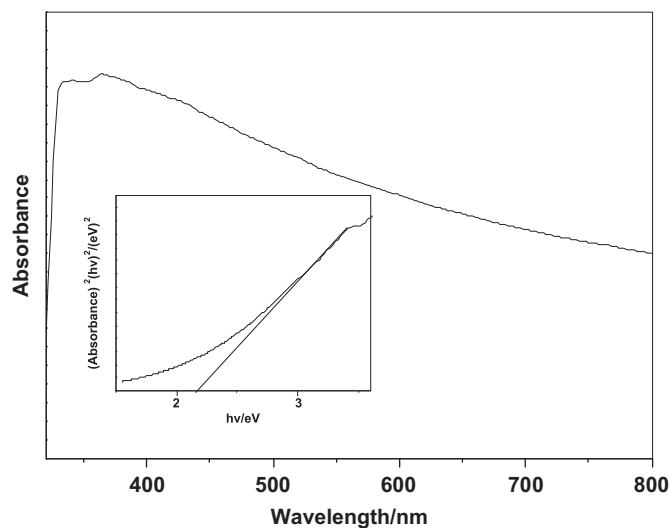
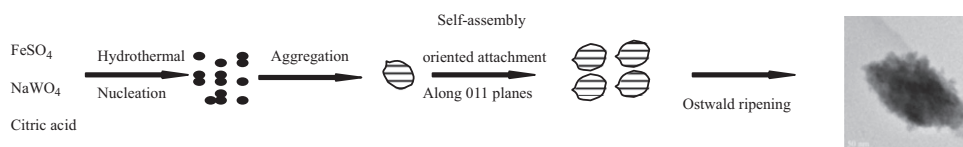


Fig. 5. Typical UV–Vis spectra of the spindle-like FeWO_4 nanoparticles.



Scheme 1. A schematic illustration of the formation mechanism of monodisperse spindle-like nanoparticles.

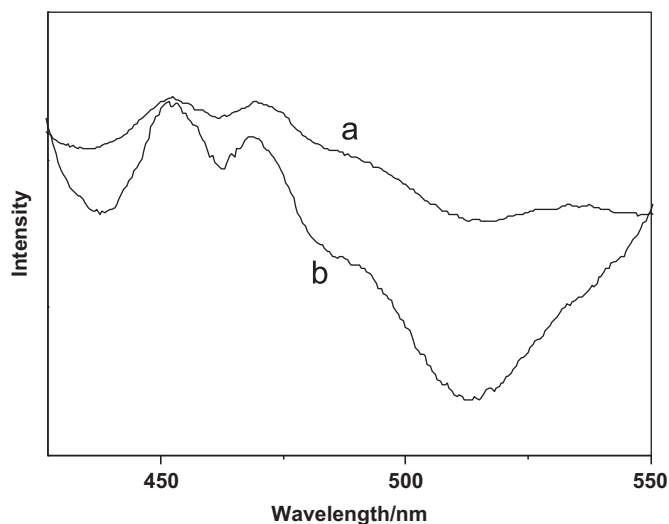


Fig. 6. Room temperature photoluminescence spectra of the FeWO_4 samples prepared under different pH values: (a) pH=7, (b) pH=8. All the photoluminescence spectra are excited with 300 nm photos.

to a light yellow, and then to transparent, which can be observed by the naked eye, suggesting the complete photocatalytic decolorization of MO aqueous solution during the reaction.

To reveal the photocatalytic activity of the spindle-like FeWO_4 nanoparticles, the MO photodegradation test with normal photocatalysts TiO_2 (P-25) has also been performed for comparison. The temporal evolution of the absorption spectra with the presence of P-25 was shown with white hollow triangles in Fig. 7a. In this figure, the absorption spectra of these two solutions are overlap when the experiments just begin. With the irradiation time increasing, the absorption peak intensity of these two solutions decreased. But every line of absorption spectra with FeWO_4 decreases faster than its corresponding line of P-25, which means that spindle-like FeWO_4 nanoparticles show better photocatalytic activities than P-25. For example, the intensity of absorption spectra of FeWO_4 at 20 min is even lower than that of P-25 at 30 min.

Another FeWO_4 sample obtained at pH 8 was also employed as photocatalysts for photodegradation of MO to investigate the relationship of the sample's morphology and its photocatalytic efficiency. The results of the MO degradation with different photocatalysts were concluded in Fig. 7b. The blank test (curve D) displays that the degradation of MO can be ignored after 50 min of UV irradiation without photocatalyst, indicating that FeWO_4 photocatalyst is the key factor in the photodegradation of MO. Curve A and B show that the photodegradation was apparently enhanced, when the FeWO_4 photocatalysts obtained under different pH values were dispersed in MO solutions. After exposure under UV light for 30 min, 74% of MO molecules were degraded with monodisperse spindle-like FeWO_4 photocatalysts, and the decomposition efficiency increased to 91% after 50 min. After 30 min and 50 min UV irradiation with FeWO_4 particles obtained under pH 8, the decomposition efficiency is 57% and 81%, respectively. As for P-25 photocatalysts, the decomposition efficiency is 56% for 30 min and 85% for 50 min. The monodisperse spindle-like FeWO_4 particles show higher photocatalytic efficiency for the degradation of MO than irregular FeWO_4 particles and normal TiO_2 . The enhanced photocatalytic activity of monodisperse spindle-like FeWO_4 particles should be attributed to more defects and higher surface area which is derived from its monodisperse spindle-like structures. This result is consistent with the conclusion drawn from the PL spectra. This

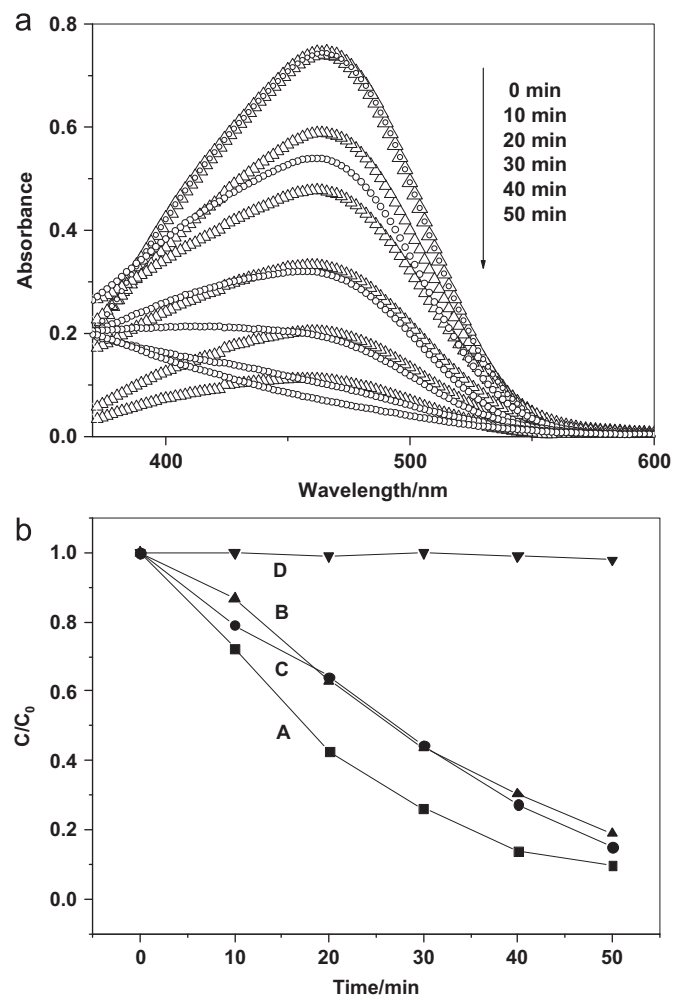


Fig. 7. (a) The temporal evolution of the absorption spectra of the MO solution in the presence of monodisperse spindle-like FeWO_4 nanoparticles (white hollow circle) and P-25 TiO_2 (white hollow triangle) under exposure of UV light. (b) Photodegradation of MO (10 mg/L, 100 mL) with different FeWO_4 samples as photocatalysts: (A) with monodisperse spindle-like FeWO_4 nanoparticles obtained under pH 7, (B) with irregular FeWO_4 nanoparticles obtained under pH 8 (C) with TiO_2 (P-25), and (D) without photocatalysts.

experimental result demonstrates that the photocatalytic activity of FeWO_4 photocatalysts is susceptible to their morphology.

Thermal stability is the key role for the recycled application of the photocatalyst. The monodisperse spindle-like FeWO_4 nanoparticles are very stable and cannot be broken into individual particles even after ultrasonication for 1 h. The catalytic activities of FeWO_4 were measured by the photodegradation of MO for five cycles. It is shown in Fig. 8 that the catalytic activity displays no significant decrease after five cycles. It is indicated that the stability of monodisperse spindle-like FeWO_4 is excellent and it can keep its high photocatalytic activity after the photocatalytic reaction and recycling process. After reused for five cycles, this kind of photocatalysts was subjected to be characterized with the XRD, SEM and TEM techniques in order to detect the possible changes in crystal structure and morphology. It was indicated that the crystal structure and morphology of the reused spindle-like FeWO_4 nanoparticles remained.

4. Conclusions

In summary, a surfactant-assisted hydrothermal method was developed to synthesize monodisperse spindle-like FeWO_4

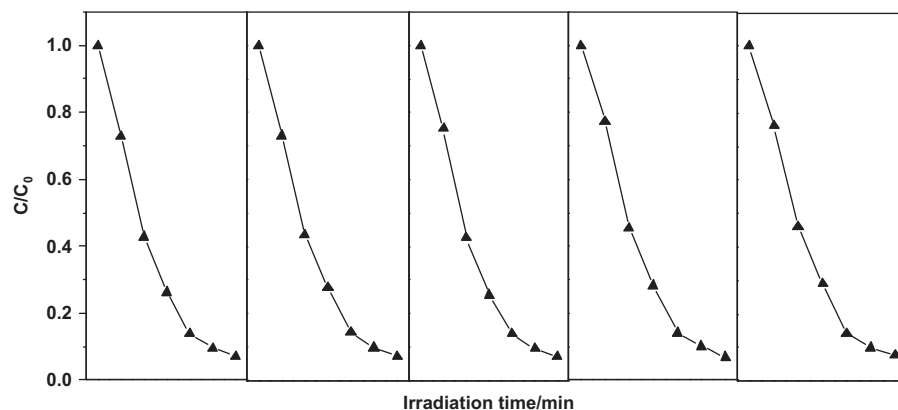


Fig. 8. Cycling runs of photodegradation of MO in the presence of monodisperse spindle-like FeWO₄ nanoparticles.

nanoparticles. It is found that the presence of citric acid is essential for the formation of such specific FeWO₄ morphology. The pH values appear to play a determining role in the morphological construction of monodisperse spindle-like FeWO₄ nanoparticles. The growth mechanism for this monodisperse spindle was proposed as a combination of the initial aggregation of nuclei adhered with citric acid, an oriented self-assembly attachment of nanobuilding particles and the Ostwald ripening progress. It is interesting that the PL spectra of monodisperse spindle-like FeWO₄ nanoparticles shows higher emission intensity at the position of 469 nm than that of ordinary FeWO₄ sample obtained at pH 8, which is related to higher surface area and more defects of monodisperse spindle-like nanoparticles. And the band gap energy of the monodisperse spindle-like FeWO₄ nanoparticles was estimated to be about 2.17 eV with UV–Vis spectra. The monodisperse spindle-like FeWO₄ nanoparticles exhibited excellent photocatalytic activity and good stability for the photodegradation of MO. This unique form of FeWO₄ microstructure may find applications in decontamination field.

Acknowledgments

We gratefully acknowledge for the National Natural Science Foundation of China (21003079), Research Award Fund for Outstanding Middle-Aged and Young Scientist of Shandong Province (BS2011CL020), Natural Science Foundation of Shandong Province (ZR2011BM018), Taishan Scholar Foundation of Shandong Province (ts20070713), Qingdao Project of Science and Technology (12-1-4-3-(20)-jch), (11-2-4-3-(16)-jch) for the financial support.

References

- [1] Y. Tian, C. Shen, C. Li, X. Shi, Y. Huang, H. Gao, Nano Res. 4 (2011) 780–787.
- [2] M. Deng, Y. Ma, S. Huang, G. Hu, L. Wang, Nano Res. 4 (2011) 685–694.
- [3] M.L. Ambrosi, R. Dei Giorgi, C. Neto, P. Baglioni, Langmuir 17 (2001) 4251–4255.
- [4] X. Liu, J. Lin, J. Nanopart. Res. 9 (2007) 869–875.
- [5] G. Liu, X. Li, X. Dong, J. Wang, J. Nanopart. Res. 13 (2011) 4025–4034.
- [6] X.H. Li, C.L. Xu, X.H. Han, L. Qiao, T. Wang, F.S. Li, Nanoscale Res. Lett. 5 (2010) 1039–1044.
- [7] S.J. Han, K. Shin, K.D. Suh, J.H. Ryu, Macromol. Res. 16 (2008) 399–403.
- [8] S. Ghost, D. Divya, K.C. Remani, T.S. Sreeremya, J. Nanopart. Res. 12 (2010) 1905–1911.
- [9] H. Wang, T. Nann, Nanoscale Res. Lett. 6 (2011) 267–272.
- [10] T.J. Daou, G. Pourroy, S. Bégin-Colin, J.M. Grenèche, C. Ulhaq-Bouiller, P. Legare, P. Bernhardt, C. Leuvrey, G. Rogez, Chem. Mater. 18 (2006) 4399–4404.
- [11] D. Chen, G. Zhu, X. Zhu, X. Qiao, J. Chen, J. Mater. Sci. - Mater. Electron. 22 (2011) 1788–1795.
- [12] G.R. Yi, J.H. Moon, V.N. Manoharan, D.J. Pine, S.M. Yang, J. Am. Chem. Soc. 124 (2002) 13354–13355.
- [13] J.P. Rolland, B.W. Maynor, L.E. Euliss, A.E. Exner, G.M. Dension, J.M. DeSimone, J. Am. Chem. Soc. 127 (2005) 10096–10100.
- [14] C.H. Choi, J.H. Jung, T.S. Hwang, C.S. Lee, Macromol. Res. 17 (2009) 163–167.
- [15] S.H. Yu, B. Liu, M.S. Mo, J.H. Huang, X.M. Liu, Y.T. Qian, Adv. Funct. Mater. 13 (2003) 639–647.
- [16] M. Cheng, Y. Liu, Y. Xiao, Y. Zhu, Q. Guan, D. Yuan, J. Zhang, J. Phys. Chem. C 113 (2009) 8455–8459.
- [17] Z. Yang, D. Han, D. Ma, H. Liang, L. Liu, Y. Yang, Cryst. Growth Des. 10 (2010) 291–295.
- [18] Q. Zhang, W.T. Yao, X. Chen, L. Zhu, Y. Fu, G. Zhang, L. Sheng, S.H. Yu, Cryst. Growth Des. 7 (2007) 1423–1431.
- [19] F. Amano, K. Nogami, R. Abe, B. Ohtani, J. Phys. Chem. C 112 (2008) 9320–9326.
- [20] X. Guo, J. Yang, Y. Deng, H. Wei, D. Zhao, Eur. J. Inorg. Chem. (2010) 1736–1742.
- [21] X.J. Dai, Y.S. Luo, W.D. Zhang, S.Y. Fu, Dalton Trans. 39 (2010) 3426–3432.
- [22] W. Hu, Y. Zhao, Z. Liu, C.W. Dunnill, D.H. Gregory, Y. Zhu, Chem. Mater. 20 (2008) 5657–5665.
- [23] Y.X. Zhou, H.B. Yao, Q. Zhang, J.Y. Gong, S.J. Liu, S.H. Yu, Inorg. Chem. 48 (2009) 1082–1090.
- [24] Q. Zhang, X. Chen, Y. Zhou, G. Zhang, S.H. Yu, J. Phys. Chem. C 111 (2007) 3927–3933.
- [25] J. Zhang, Y. Wang, S. Li, X. Wang, F. Huang, A. Xie, Y. Shen, Cryst. Eng. Commun. 13 (2011) 5744–5750.
- [26] J.F. Banfield, S.A. Welch, H.Z. Zhang, T.T. Ebert, R.L. Penn, Science 289 (2000) 751–754.
- [27] C. Murphy, Science 298 (2002) 2139–2141.
- [28] T. Ejima, T. Banse, H. Takatsuka, Y. Kondo, M. Ishino, N. Kimura, M. Watanabe, I. Matsubara, J. Lumin. 119 (2006) 59–63.
- [29] M. Niklm, Phys. Status Solidi A 178 (2000) 595–620.